High Orientation of Long chain branched Poly (lactic acid) with Enhanced Blood Compatibility and Bionic Structure

[1]Zhengqiu Li, [1]Lin Ye, [1]Xiaowen Zhao*, [2]Phil Coates, [2]Fin Caton-Rose, [2]Michasel Martyn

1. State Key Laboratory of Polymer Materials Engineering of China, Polymer Research Institute of Sichuan University, Chengdu, China

2. School of Engineering, Design and Technology, University of Bradford, Bradford, U.K.

*Corresponding author. Tel.: 862885408802; Fax: 862885402465. E-mail address: zhaoxiaowenscu@126.com

Abstract: Highly-oriented poly (lactic acid) (PLA) with bionic micro-grooves was fabricated through solid hot drawing technology for further improving the mechanical properties and blood biocompatibility of PLA. In order to enhance the melt strength and thus obtain high orientation degree, long chain branched PLA (LCB-PLA) was prepared at first through a two-step ring-opening reaction during processing. Linear viscoelasticity combined with branch-on-branch (BOB) model was used to predict probable compositions and chain topologies of the products, and it was found that the molecular weight of PLA increased and topological structures with star like chain with three arms and tree-like chain with two generations formed during reactive processing, and consequently draw ratio as high as1200% can be achieved during the subsequent hot stretching. With the increase of draw ratio, the tensile strength and orientation degree of PLA increased dramatically. Long chain branching and orientation could significantly enhance the blood compatibility of PLA by prolonging clotting time and decreasing platelet activation. Micro-grooves can be observed on the surface of the oriented PLA which were similar to the intimal layer of blood vessel, and such bionic structure resulted from the formation of the oriented shish kebab-like crystals along the draw direction.

Keywords: Poly (lactic acid) (PLA); long chain branching; mechanical properties; blood compatibility; bionic character

Introduction

Poly (lactic acid) (PLA, -[$CH(CH_3)COO]_n$-) is a linear aliphatic thermoplastic polyester which is produced from lactic acid by converting sugar or starch obtained from renewable sources (e.g., corn, wheat, or rice) [1-3]. PLA has been considered to be a good candidate for biomedical materials due to its biodegradable and biocompatible nature [4-6], and approved by the Food and Drug Administration (FDA) for numerous clinical applications, such as sutures, bone plates, abdominal mesh, and extended-release pharmaceuticals [7]. However, some problems still exist for PLA when it acts as implanted biomaterials and bio-devices: the mechanical strength of PLA is still not sufficient for weight-bearing implant fixation; the relatively poor blood compatibility of PLA may promote surface-induced thrombosis and embolization when in direct contact with blood.

Solid hot drawing technology is one of the molecular orientation methods for polymers in solid state. Through such technology, first of all, PLA with sufficient strength could be prepared to meet the requirement of desirable physical properties for biomedical use. Meanwhile, the surface properties of PLA could be changed by such processing, and thus the interaction between PLA and the biological elements of the organism might be affected.

Since large extensional deformation is encountered during the solid hot drawing processing, in order to resist rupture, moderately high elongational viscosity, high melt strength/elasticity as well as strain hardening behavior of the sample are desired. However, for neat PLA, it usually exhibits low viscosity, low melt elasticity and no strain hardening behavior as a consequence of its linear structure and a narrow molecular weight distribution, which makes it very difficult to be ultra-drawn during hot drawing [8-9].

It has been widely reported that long chain branching (LCB) had a significant effect on rheological properties of polymers, and even a small amount of LCB can lead to great increase in extensional viscosity, shear viscosity and elasticity [10-11]. Several methods have been tried to obtain PLA with long chain branched structures. L.M. Pitet et al. established a one-pot method for copolymerization of lactide with glycidol, using different temperature conditions to control the occurrence of epoxide ring opening that leads to hyperbranching [12]. Huagao Fang et al. prepared a kind of LCB-PLA by applying gamma radiation with addition of the trifunctional monomer [13]. Another convenient method to introduce LCB onto the polymer chains is to carry out the branching reactions by reactive processing in the melt state in the presence of some free-radical initiators or multifunctional chain extenders, which is evidently more convenient and cheaper and can produce a large volume of polymers. However, due to the limited end-group concentration and low activity of the end hydroxyl groups, hyperbranched structures are not easy to obtain for PLA through reactive processing.

In this work, PLA was long chain branched by ring-opening reaction with anhydride and epoxy together through reactive processing in order to enhance the molecular entanglement and melt strength of PLA. Linear viscoelasticity combined with branch-on-branch (BOB) model was used to predict probable compositions and chain topologies of the products. Then highly oriented PLA with submicrometer structures were expected to be formed through solid hot drawing technology. The structure and properties of the oriented PLA were studied, and its bionic character as well as anti-coagulation mechanism were tried to be explored.

2. Experimental Section

2.1 Materials

Poly (lactic acid) (PLA) (NatureWorks® PLA Polymer 3052D) was supplied from Nature Works in pellet form. The molecular weight (M_w) was about 1×10^5. Pyromellitic dianhydride (PMDA) (AR) was obtained from Sinopharm Chemical Reagent Co., Ltd, China. Pentaerythritol polyglycidyl ether (PGE) (AR) was obtained from Energy Chemical Co. Ltd., China.

2.2 Preparation of the highly oriented PLA

Long chain branched PLA (LCB-PLA)

After dried at 70°C for 5hrs in a vacuum oven, modification of the original PLA was conducted in a Haake internal melt mixer (Rheocord 90, Germany). After the pellets of PLA totally melted, PMDA was added to react with PLA for several minutes, and then PGE was added into the mixture. When the reaction was completed, the product was cut into small granules. The detailed formulations to prepare LCB-PLA were listed in Table 1.

Highly oriented PLA

The oriented samples of PLA and LCB-PLA were prepared by being heated and mechanically drawn. After the desired draw ratio was obtained, the sample was cooled down to room temperature, and then the load was released.

2.3 Measurements

FTIR spectroscopy

A Fourier-transform infrared spectrometer (FTIR) (Magna IR 560, Nicolet, USA) with resolution of 2 cm^{-1} was used to identify the chemical structure of the purified specimens which were prepared by grinding the powder sample with KBr to form a thin film. The scanning range was from 400 to 2000 cm^{-1}.

Dynamic Rheological Analysis

Dynamic rheological measurement was performed on an AR 1500ex dynamic stress rheometer (TA Instruments, USA). The samples were compression molded into the disk of 25 mm in diameter and around 1 mm in thickness. The measurement was run with a 25 mm-diameter parallel plate geometry and a 1.0 mm sample gap. The dynamic viscoelastic properties were determined with frequencies from 0.01 to 100 Hz at 170°C, using 1% strain (selected after strain sweep tests) value determined with a stress sweep to keep within the linear viscoelastic region. Specimens were placed between the preheated plates at the experimental temperature and were allowed to equilibrate before each run.

Two-dimensional Wide-angle X-ray diffraction analysis (2D-WAXD)

Wide-angle X-ray diffraction (WAXD) analysis was conducted at the ambient temperature using a D8 Discover two-dimensional wide angle X-ray diffractometer (2d-WAXD) (Bruker AXS Co, Germany). The sampling time of 2d-WAXD measurements was 180 s using an Eulerian 1/4 cradle HI-STAR (2D-Detector) detector, with a wavelength of 0.154 nm monochromated X-ray obtained from Cu (Kα) radiation.

Mechanical properties

The mechanical properties of PLA samples were measured with a 4302 material testing machine (Instron Co, USA) according to ISO527/1-1993 (E). The test speed was 50 mm/min, and the sample length between benchmarks was 25 mm.

Scanning electron microscope analysis (SEM)

The fractured surface morphology analysis of the samples was performed with JEOL JSM-5900LV scanning electron microscope (SEM, JEOL Co, Japan) with an acceleration voltage of 20 kV. The smooth surface was etched by a water-methanol (1:2 by volume) mixture solution containing 0.025mol/L of sodium hydroxide for 10h

at 25°C, and then the etched surface was cleaned using distilled water. The samples were sputter-coated with gold for 2~3 min.

Platelet adhesion measurement

To test the platelet adhesion, samples were incubated with the platelet rich plasma (PRP) for 1 h at 37°C under static conditions. After 1 h incubation, the samples were rinsed carefully three times with phosphate-buffered saline (PBS, pH=7.3) buffer. The adherent platelets were fixed using 2.5% glutaraldehyde in PBS for at least 1 h, dehydrated in a graded series (50%, 60%, 70%, 80%, 90%, 95%, and 100%, v/v) of ethanol, and dried under vacuum at -50°C overnight. The samples were then sputter coated with a thin layer of gold and observed using a scanning electron microscopy (JEOL JSM-5900LV).

Clotting time (APTT and TT)

Activated partial thromboplastin time (APTT) and thrombin time (TT) were measured by an automated blood coagulation analyzer CA-50 (Sysmex Corporation, Kobe, Japan), and the test method was described as follows: fresh blood was collected using vacuum tubes, containing sodium citrate as an anticoagulant (anticoagulant to blood ratio, 1:9, v/v). The platelet-poor plasma (PPP) was obtained after centrifuging at 4000 rpm for 15 min. Synchronously, the samples (0.4 cm×0.5 cm) were immersed in PBS (0.2 mL, pH = 7.4) for 1 h. Then the PBS was removed and 0.1 mL of fresh PPP was introduced. After incubating at 37°C for 30 min, 50μL of the incubated PPP was added into the test cup, followed by the addition of 50μL of APTT agent (incubated 10 min before use) and incubation at 37°C for 3 min. Thereafter, 50μL of 0.025 M $CaCl_2$ solution was added, and then the APTT was measured. For the TT test, 50μL of TT agent was added into the test cup (containing 50μL of the incubated PPP) after 10 min incubating, and then the TT was measured. At least three measurements

were averaged to get a reliable value, and the results were analyzed by statistical method.

Statistical analysis

The quantitative results were obtained from triplicate samples and the data was expressed as mean ± SD (n = 3 or 5). Statistical analysis was performed using one-way analysis of variance, followed by post hoc Student's t-test. A value of $p < 0.05$ was considered to be statistically significant.

3. Results

3.1 Characterization of LCB-PLA

FTIR spectra of PGE, pure PLA, purified PLA-PGE and LCB-PLA-5 were shown in Fig. 1(a). The dash line in the figure guided the two transmission peaks at 928 cm^{-1} and 1107 cm^{-1}, which were attributed to the asymmetrical stretching vibration of C-O-C (epoxy group) and characteristic stretch absorption of C-O-C (ether) respectively on PGE molecule [14-15]. These two peaks could not be clearly observed for sample PLA-PGE, however, the peak at 1107 cm^{-1} for sample LCB-PLA-5 could be clearly observed which indicated that PGE was grafted onto the PLA chains successfully by introducing PMDA. Moreover, a slight absorbance at 928 cm^{-1} attributed to epoxy groups still can be observed for sample LCB-PLA-5 indicating that not all of the four epoxy groups on PGE participated in the branching reaction.

Torque evolution during the branching reactions was shown in Fig. 1(b). The torque of neat PLA decreased monotonously with the mixing time, which was ascribed to the possible thermal degradation of PLA during processing. For PLA branched by PMDA or PGE independently, no obvious increase of torques could be

observed, which should be attributed to the low extending or branching degree of PLA chains. In contrast, the torque showed completely different trend when the sample reacted with both PMDA and PGE, which climbed steeply until it reached a plateau in about 35 min.

The basic idea of branch-on-branch (BOB) model is the hierarchical relaxation of branched structures. It has been shown that BOB model could predict the linear viscoelasticity of branched chains quite satisfactorily when compared with the experiments of model branching polymers. The details of the model and algorithm would not be repeated here and can be found in the original publication [16-17]. The BOB model was tried here to find out the compositions and chain structures of PLA and LCB-PLA, which could be done by fitting the experimental data, i.e., dynamic modulus and complex viscosity, with the model predictions.

Characteristic parameters for PLA used in BOB model were as follows: density was 1.24 g/cm^3; the number of monomer in one entangled segment was 110; and the entanglement time τ_e was 10^{-5} s. The BOB fitting results of linear viscoelasticity for the linear PLA before branching were shown in Fig. 2(a). The weight average molecular weight ($\overline{M_w}$) was fitted to be 100 kg/mol and the polydispersity index (PDI, defined as the ratio between the weight average molecular weight and the number average molecular weight) was 1.2 where the molecular weight distribution was assumed to follow log-normal distribution. The molecular weight and its distribution obtained from fitting linear viscoelasticity were quite close to those measured by GPC.

For PLA after branching, it was assumed that the branched products were composed of linear, symmetric-star, asymmetric-star, H-type, pom-pom, comb and tree-like chains. Therefore, the parameters for the molecular structures, such as

volume fraction, molecular weight and its distribution, arm length, could be obtained by fitting the experimental data with BOB model. The fitting results for LCB-PLA samples were shown in Fig. 2(b-f). The structure parameters obtained from fitting were listed in Table 2, which revealed the most possible chain topology of samples.

3.2 Orientation and mechanical properties of LCB-PLA

The increase of molecule weight and the successful formation of long chain branched structure for LCB-PLA encouraged us to perform solid hot drawing processing on them. For neat PLA, the maximum draw ratio was about 600%, while for LCB-PLA, with increasing chain extender content, the maximum draw ratio initially increased and then declined somewhat. The maximum draw ratio can reach up to 1200% for LCB-PLA-3 due to its proper fraction of the branched chain (as shown in Fig. 3(b)).

The XRD patterns of PLA and LCB-PLA-3 before and after drawing were shown in Fig.4(a). The isotropic sample did not show any Debye-Scherrer diffraction rings due to its low crystallinity and the random arrangement of grains. While for the samples after drawing, the (200)/(110) reflection appeared as two strong circular spots on the equator and a four-point image formed by (203) reflection. With increasing draw ratio, these arcs became narrower in spread and more prominent, suggesting that the crystal axis was preferentially oriented parallel to the draw direction. The crystallinity of PLA and LCB-PLA-3 can be calculated by the peak area of crystal and amorphous region from the corresponding decomposed curves obtained by Peak Fit software. The orientation parameter (f) was calculated using Herman's orientation function:

$$f = \frac{3\left\langle \cos^2 f \right\rangle - 1}{2} \quad (1)$$

$$\left\langle \cos^2 \phi \right\rangle = \frac{\int_0^{\pi/2} I(\phi) \sin\phi \cos^2\phi \, d\phi}{\int_0^{\pi/2} I(\phi) \sin\phi \, d\phi} \quad (2)$$

Where I(ϕ) is the scattering intensity along the angle ϕ. When taking ϕ = 0 as the shear flow direction, the critical values of fare −0.5 for a perfect perpendicular orientation, 0 for a random orientation and 1 for a perfect parallel orientation, respectively. The orientation factor and crystallinity were summarized in Fig.3 (b). With the increase of draw ratio, the orientation factor and crystallinity of PLA and LCB-PLA-3 increased.

The mechanical properties of PLA and LCB-PLA-3 with different draw ratio were shown in Fig.4 (c). Before orientation, compared to the neat PLA, long chain branching did not bring about remarkable change in tensile strength and modulus. With increasing draw ratio, the tensile strength and modulus increased sharply, and at 1200% of drawing ratio, the tensile strength and the tensile modulus of LCB-PLA-3 reached up to 170±6 MPa and 6.7±0.3 GPa, respectively.

3.3 Blood compatibility of oriented LCB-PLA

The platelet adhesion densities on the samples were evaluated, as shown in Fig.5. After contacting with platelet-rich plasma (PRP) for 60 min, a large number of platelets were observed to aggregate on the surface of isotropic PLA. In the case of LCB-PLA-3, however, the surface seemed prone to prevent platelets from adhering, since much fewer platelets were observed. Moreover, with increasing draw ratio, platelet adherent density on LCB-PLA-3 was further significantly reduced and platelets on oriented samples almost remained their original shape.

Fig.6 showed APTT and TT of neat PLA and LCB-PLA-3. For the APTT tests, the blood clotting time of PLA (39.1±1.3 s) increased compared with the control (37.5±1.1 s), and the APTTs of the LCB-PLA-3 (50.1±1.3 s) were much longer compared with the neat PLA. After orientation, the APTTs increased further with the increase of draw ratio, and the blood clotting time of LCB-PLA-3-1200% was prolonged to 97±1.2s. The values of TT also increased slightly after long chain branching and stretching.

4. Discussion

The results of FTIR indicated that large amount of PGE cannot be easily grafted on PLA chains directly. Although epoxy groups can react with both terminal carboxyl and terminal hydroxyl groups of polyester, the reactivity of epoxy with carboxyl group was higher than that with hydroxyl group [18]. Moreover, the concentration of carboxyl groups on PLA chains was very low as the terminal carboxyl groups might be end-capped for pure PLA. Therefore, to improve the grafting ratio of PGE, PMDA was introduced at first and then LCB-PLA could be prepared successfully.

Since the torque value was proportional to the apparent viscosity of materials, which depended on the molecular weight and chain structure of the polymer, the dramatic increase of torque certainly indicated the formation of the long polymer chains or high chain branching in reaction system. The obviously increasing torques for LCB-PLA-2~5 should be a result of two-step reaction of PLA with PMDA and then with PGE, which led to a remarkable increase in the molecular weight and the formation of branching structure.

According to the results of BOB model, as shown in Fig. 2(b-f), the fitted lines were quite closed to the experimental data when assuming that all products branched

with varying contents of chain extender were just composed of linear, star like chain with 3 arms and tree-like chain with two generations molecules. On the basis of the structure parameters listed in Table 2, it can be seen that the linear chains in different LCB-PLA samples presented different molecular weight ($\overline{M_w}$), because chains experienced both extension and degradation. All LCB-PLA samples exhibited higher $\overline{M_w}$ of linear chains compared with pure PLA, implying that the chain extension was certainly able to compensate the decrease in average molecular weight due to degradation. With increasing chain extender content, the volume fraction of the linear chain component decreased, while the fraction of the branched chain including star like and tree-like chain component increased.

Based on the data of XRD, it indicated that slipping and rupture of the lamellar in the spherulite occurred during the drawing of PLA and a clear orientation of PLA molecules formed, which induced the dramatic increase of the tensile strength and modulus of PLA.

When platelets were activated, they will deform and crosslink to promote aggregation of further platelets. Platelet adhesion and activation on the surface of a biomaterial was the most essential character in determining the blood compatibility of a biomaterial. Low platelet adhesion and activation denotes good blood compatibility, while a higher degree of platelet adhesion and activation could result in a thrombus. Fewer platelets adhesion on the surface of oriented long chain branched sample indicated that the activation of platelets activation of the intrinsic blood coagulation system was suppressed.

The APTT (activated partial thromboplastin time) and TT (thrombin time) tests are widely used for the clinical detection of the abnormality of blood plasma and the primary screening of the anticoagulative chemicals and they are recently applied in

the evaluation of the in vitro antithrombogenicity of biomaterials. In general, APTT was used to measure the inhibited efficacy of both the intrinsic (or referred to as the contact activation pathway) and the common plasma coagulation pathways including factors II, V, X, XII or fibrinogen [19]. TT was used to measure the clot formation time for the thrombin to convert fibrinogen into fibrin in the platelet-poor plasma (PPP). The shorter clotting time indicates the faster conversion of fibrinogen to insoluble fibrin protein, which then leads to thrombus [20]. Therefore, the obviously shorter APTT indicated that the chain branching and orientation had significant effect on inhibiting the intrinsic and the common plasma coagulation pathways of coagulation.

From the material science point of view, a native blood vessel was the best blood compatible material [21]. The intimal layer of the blood vessel can resist platelet adhesion and prevent undesirable thrombus formation. When the surface roughness was within the range of 50 nm (dimension of proteins) to 2 μm (dimension of platelets), particular surface topographies, such as grooves, may reduce the contact area for platelets, which can only adhere on the top of the topographic features, platelet adhesion and thrombus formation may thus be reduced. A variety of methods including mechanical and electrochemical, polishing/roughening, chemical etching and different patterning strategies (lithography, molding, embossing, imprinting, self-assembly), have been investigated for the fabrication of such surface topography [22].

The surface morphology of LCB-PLA before and after orientation were investigated with SEM and AFM, which were shown in Fig.7 (a). Before orientation, the surface architectures of LCB-PLA were smooth and flat. After orientation, the surfaces with alternating parallel grooves and ridges at the sub-micron scale can be

observed. The average width of the ridges was about 500nm and the height was about 100 nm. These particular parallel grooves and ridges at the sub-micron scale were similar in size to that of the inner surface of blood vessels. It was very exciting that self-reinforced PLA with vessel-like bionic surface could be fabricated by solid hot stretching technology.

To explore the formation mechanism of bionic structure through processing, the morphology of etched LCB-PLA were investigated with SEM. The smooth surface was etched by a water-methanol (1:2 by volume) mixture solution containing 0.025mol/L of sodium hydroxide for 10h at 25°C to remove the amorphous parts of PLA. As shown in Fig. 7(b), some imperfect stacking of spherulite structures were observed for LCB-PLA before orientation, with the lath-like lamellae arranged irregularly. However, for highly oriented sample, the oriented shish kebab-like crystals appeared along the draw direction. During the solid hot drawing process, high-molecular weight fraction of LCB-PLA oriented and self-organized into fibrils which were capable of serving as shish to induce the epitaxial growth of kebab-like lamellae approximately orthogonal to their long axis. Therefore, the oriented LCB-PLA surface showed a preferential orientation grooves as shown in Fig. 7 (a).

5. Conclusions

Highly-oriented LCB-PLA with enhanced mechanical properties and improved blood compatibility were fabricated through solid hot drawing technology. FTIR and BOB model was used to confirm the structure of the LCB-PLA, indicating that PLA branched with PMDA and PGE together were made of linear, star-like and tree-like chains with two generations. The melt strength and molecular entanglement were enhanced by long chain branching and thus higher draw ratio can be achieved. The tensile strength and orientation degree of PLA increased dramatically with the

increase of draw ratio. The results of in vitro blood compatibility showed that, compared with neat PLA, oriented samples after long chain branching exhibited less platelet adhesion and longer clotting time, indicating that the samples with highly molecular orientation exhibited an appreciably better blood compatibility than neat PLA. Submicrometer structures including alternating parallel grooves and ridges at the micron scale which were similar to intimal layer of blood vessel can be observed for the oriented PLA. These submicrometer structures were formed due to the shish kebab-like crystals after orientation.

Acknowledgements

This research was supported by National Natural Science Foundation of China (Grant No. 51303109), International Scientific and Technological Cooperation Project of Sichuan Province (Grant No. 2015HH0019) and Fundamental Research Funds for the Central Universities (Grant No. 2015SCU04A27).

References

[1] R. Babu, R. Seeram, Current progress on bio-based polymers and their future trends, Progress in Biomaterials, 2 (2013) 8-24.

[2] L. T. Sin, A.R. Rahmat, WAWA Rahman, Polylactic acid: PLA biopolymer technology and applications, Elsevier, Oxford, UK, 2012.

[3] C. Vilela, A.F. Sousa, A.C. Fonseca, A.C. Serra, The quest for sustainable polyesters-insights into the future, Polymer Chemistry, 5 (2014) 3119-3141.

[4] I. Armentano, N. Bitinis, E. Fortunati, S. Mattioli, Multifunctional nanostructured PLA materials for packaging and tissue engineering, Progress in Polymer Science, 38 (2013) 1720-1747.

[5] C Xie, H Lu, W Li, FM Chen, YM Zhao, The use of calcium phosphate-based

biomaterials in implant dentistry, Journal of Materials Science: Materials in Medicine, 23 (2012) 853-862.

[6] F. Mai, Y. Habibi, J.M. Raquez, P. Dubois, J.F. Feller, Poly (lactic acid)/carbon nanotube nanocomposites with integrated degradation sensing, Polymer, 54 (2013) 6818-6823.

[7] E. Lizundia, E. Meaurio, J.M. Laza, J.L. Vilas, L.M. León Isidro, Study of the chain microstructure effects on the resulting thermal properties of poly(L-lactide)/poly(N-isopropylacrylamide) biomedical materials, Materials Science and Engineering: C, 50 (2015) 97-106.

[8] M. Katherine Dean, E. Petinakis, S. Meure, L. Yu, A. Chryss, Melt Strength and Rheological Properties of Biodegradable Poly(Lactic Aacid) Modified via Alkyl Radical-Based Reactive Extrusion Processes, J Polym Environ, 20 (2012) 741-747.

[9] H. Tang, W. Dai, B. Chen, A New Method for Producing High Melt Strength Polypropylene With Reactive Extrusion, Polymer engineering and science, 48 (2008) 1339-1344.

[10] J. Liu, L. Lou, W. Yu, R. Liao, R. Li, C. Zhou, Long chain branching polylactide: Structures and properties, Polymer, 51 (2010) 5186-5197.

[11] J. Liu, S. Zhang, L. Zhang, Y. Bai, Preparation and rheological characterization of long chain branching polylactide, Polymer, 55 (2014) 2472-2480.

[12] L.M. Pitet, S.B. Hait, T.J. Lanyk, D.M. Knauss. Linear and Branched Architectures from the Polymerization of Lactide with Glycidol, Macromolecules, 40 (2007) 2327-2334.

[13] H. Fang, Y. Zhang, J. Bai, Z. Wang, Z. Wang, Bimodal architecture and rheological and foaming properties for gamma-irradiated long-chain branched polylactides, RSC Advances, 3 (2013) 8783-8795.

[14] X. Gua, X. Huang, H. Wei, X. Tang, Synthesis of novel epoxy-group modified phosphazene-containing nanotube and its reinforcing effect in epoxy resin, 47 (2011) 903-910.

[15] B Gupta, N Revagade, J Hilborn, Poly (lactic acid) fiber: an overview, Progress in polymer science, 32 (2007) 455-482.

[16] D.J. Read, D. Auhl, C. Das, J. den Doelder, M. Kapnistos, Linking models of polymerization and dynamics to predict branched polymer structure and flow, Science, 333 (2011) 1871-1874.

[17] B. Mallet, K. Lamnawar, Improvement of blown film extrusion of poly(Lactic Acid): Structure-Processing-Properties relationships, Polymer Engineering and science, 54 (2014) 840-857.

[18] C. Das, N.J. Inkson, D.J. Read, Computational linear rheology of general branch-on-branch polymers, Journal of Rheology, 50 (2006) 207-235.

[19] L. L. K. Leung, ASH Education Program Book, 2006, 457-461.

[20] M.M. Flanders, R. Crist, G.M. Rodgers, Comparison of five thrombin time reagents, Clin. Chem., 49 (2003), 169-172.

[21] X. Liu, L. Yuan, D. Li, Z. Tang, Y. Wang, G. Chen, Blood compatible materials: state of the art, J. Mater. Chem. B, 2 (2014), 5718-5738.

[22] H. Fan, P. Chen, R. Qi, J. Zhai, D. Han, L. Jiang, Greatly improved blood compatibility by microscopic multiscale design of surface architectures, Small,

19 (2009) 2144–2148.

Table caption

Table 1 The formulations for PLA and LCB-PLA samples.

Table 2 The structure parameters of LCB-PLA obtained from BOB model.

Table 1. The formulations for PLA and LCB-PLA samples

Samples	PMDA (wt%)	PGE (wt%)
PLA	0	0
PLA-PGE	0	1
PLA-PMDA	1	0
LCB-PLA-1	0.1	0.1
LCB-PLA-2	0.3	0.3
LCB-PLA-3	0.5	0.5
LCB-PLA-4	0.7	0.7
LCB-PLA-5	1	1

Table 2 The structure parameters of LCB-PLA obtained from BOB model

Samples	η_0 (*10^3 Pa.s)	Linear chain		Star like chain with 3 arms		Tree-like chain with two generations		
		ψ	M_w/PDI	ψ	M_a/PDI	ψ	M_{g0}/PDI	M_{g1}/PDI
PLA	0.93	1	100/1.2	--	--	--	--	--
LCB-PLA-1	2.34	0.98	120/1.2	0.01	110/1.2	0.01	50/1.0	220/1.0
LCB-PLA-2	6.24	0.9	160/1.2	0.05	120/1.2	0.05	50/1.0	220/1.0
LCB-PLA-3	21.5	0.84	240/1.2	0.08	120/1.2	0.08	100/1.0	240/1.0
LCB-PLA-4	139	0.8	220/1.2	0.1	120/1.2	0.1	100/1.0	240/1.0
LCB-PLA-5	256	0.75	200/1.2	0.15	120/1.2	0.1	100/1.0	240/1.0

a. ψ stands for volume fraction of the corresponding component.

b. M_w and Ma are the molecular weight of backbone and side arm, respectively; M_{g0} and M_{g1} are the molecular weight of the generation zero and one for tree-like chains, respectively. The unit for all molecular weights listed above is kg/mol.

Figure captions

Figure 1 (a) FTIR spectra (825-1175 cm^{-1}) of PGE, pure PLA, PLA-PGE and LCB-PLA; **(b)** Torque evolutions during the branching reactions.

Figure 2 Linear viscoelastic spectra at 170°C for **(a)** pure PLA; **(b)** LCB-PLA-1; **(c)** LCB-PLA-2; **(d)** LCB-PLA-3; **(e)** LCB-PLA-4; **(f)** LCB-PLA-5. (Square □ and circular ○ were the experimental SAOS data, and lines were the results of simulation).

Figure 3 (a) The reactive processing conducted in the Haake internal melt mixer and the mechanism of the branching reactions; **(b)** Chain structure and solid hot drawing of LCB-PLA-3.

Figure 4 (a) Two-dimensional XRD patterns of PLA and LCB-PLA-3 with different draw ratio; **(b)** Orientation factor and crystallinity of PLA and LCB-PLA-3 with different draw ratio; **(c)** mechanical properties of PLA and LCB-PLA-3 with different draw ratio (Values are expressed as means ± SD, n = 5).

Figure 5 Platelet adsorption of PLA and LCB-PLA-3 with different draw ratio (Magnification: 5000×) (Values are expressed as means ± SD, n = 3).

Figure 6 Clotting time of PLA and LCB-PLA-3 with different draw ratio (Values are expressed as means ± SD, n = 3).

Figure 7 (a) Formation mechanism of micro-grooves; **(b)** Bionic structure of highly oriented LCB-PLA.

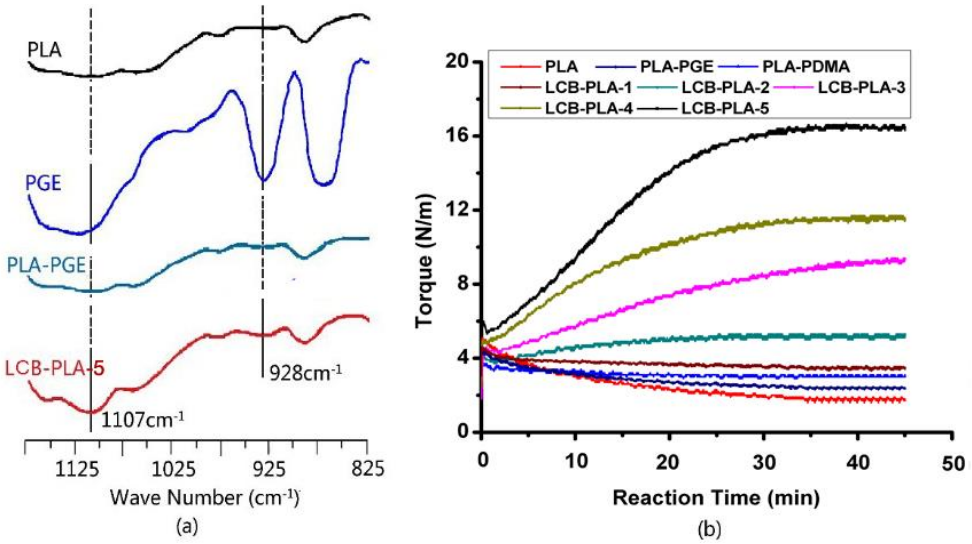

Figure 1 (a) FTIR spectra (825-1175 cm^{-1}) of PGE, pure PLA, PLA-PGE and LCB-PLA;

(b) Torque evolutions during the branching reactions.

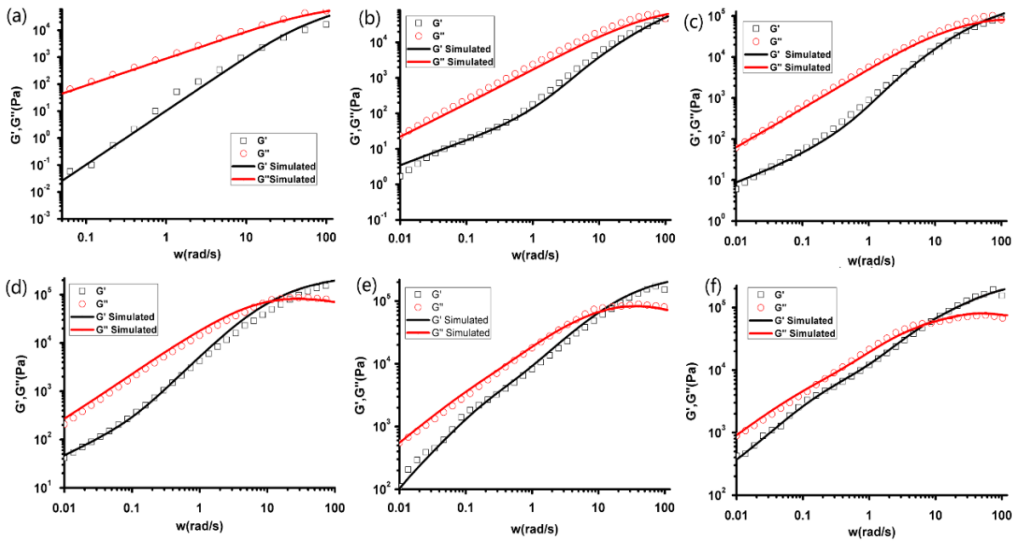

Figure 2 Linear viscoelastic spectra at 170°C for **(a)** pure PLA; **(b)** LCB-PLA-1; **(c)** LCB-PLA-2; **(d)** LCB-PLA-3; **(e)** LCB-PLA-4; **(f)** LCB-PLA-5. (Square □ and circular ○ were the experimental SAOS data, and lines were the results of simulation).

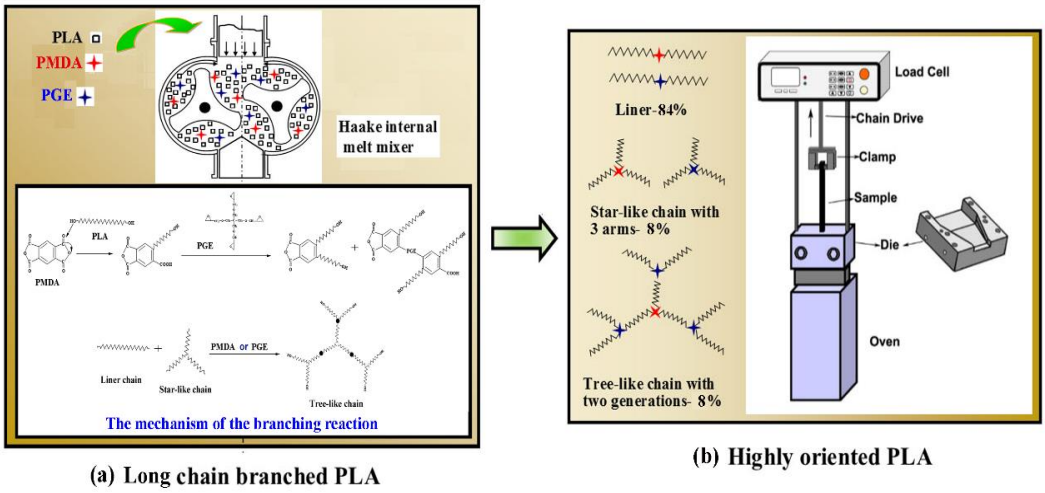

Figure 3 (a) The reactive processing conducted in the Haake internal melt mixer and the mechanism of the branching reactions; **(b)** Chain structure and solid hot drawing of LCB-PLA-3.

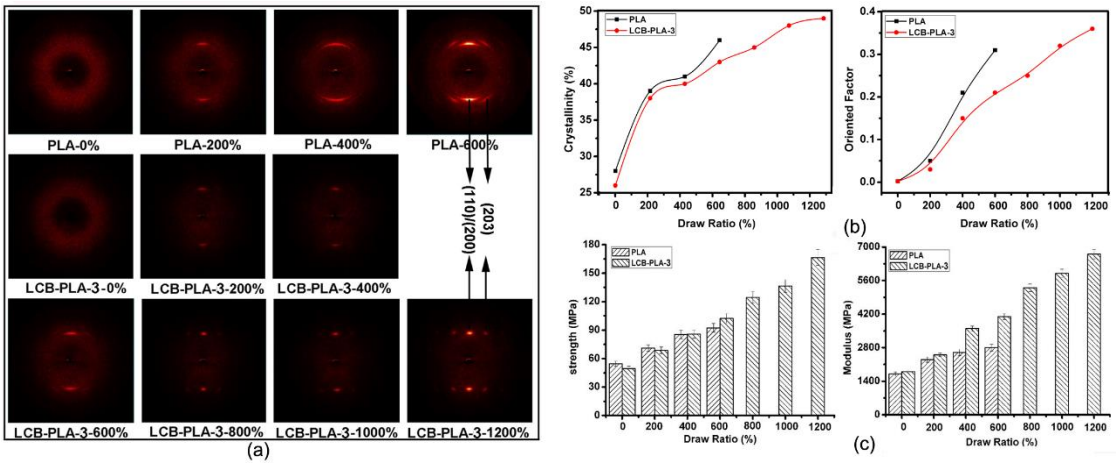

Figure 4 (a) Two-dimensional XRD patterns of PLA and LCB-PLA-3 with different draw ratio; **(b)** Orientation factor and crystallinity of PLA and LCB-PLA-3 with different draw ratio; **(c)** mechanical properties of PLA and LCB-PLA-3 with different draw ratio (Values are expressed as means ± SD, n = 5).

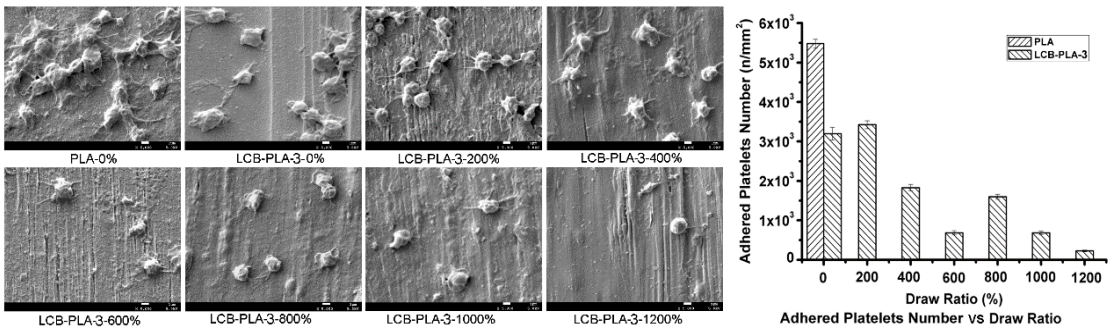

Figure 5 Platelet adsorption of PLA and LCB-PLA-3 with different draw ratio (Magnification: 5000×) (Values are expressed as means ± SD, n = 3).

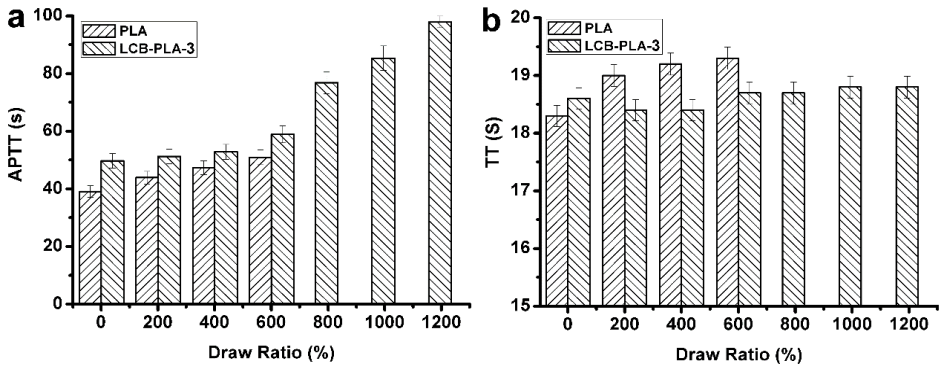

Figure 6 Clotting time of PLA and LCB-PLA-3 with different draw ratio (Values are expressed as means ± SD, n = 3).

-

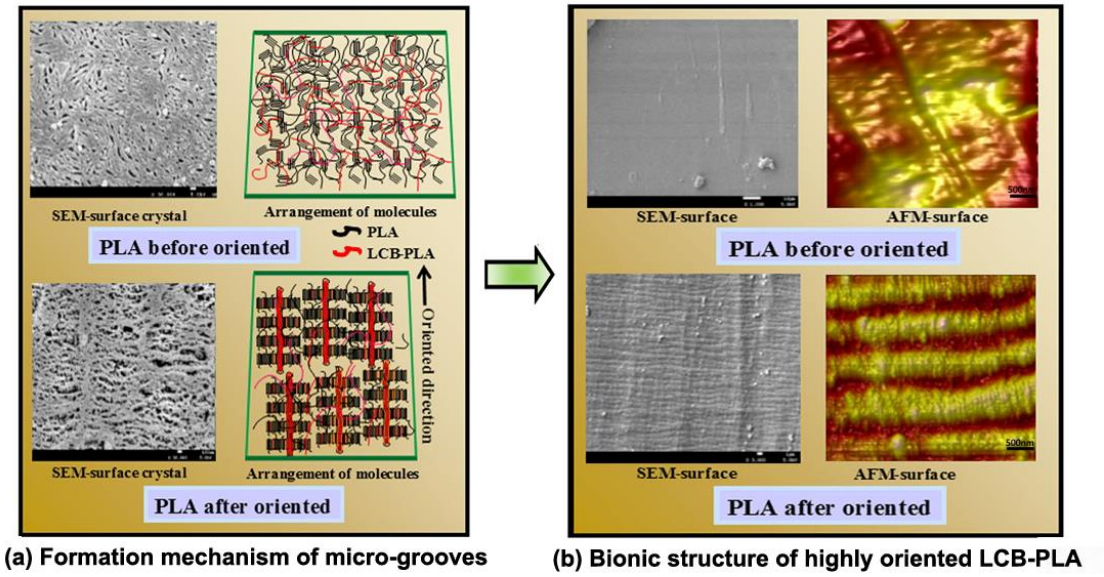

Figure 7 (a) Formation mechanism of micro-grooves; **(b)** Bionic structure of highly oriented LCB-PLA.